J Control Autom Electr Syst (2014) 25:720–731
DOI 10.1007/s40313-014-0151-5

A Methodology for Estimating Frequency Responses of Electric Power Grids

Thiago R. Oliveira · Cristiano A. G. Marques · Weiler A. Finamore · Sergio L. Netto · Moises V. Ribeiro

Received: 23 March 2014 / Revised: 14 July 2014 / Accepted: 4 September 2014 / Published online: 18 September 2014

Abstract Currently, there is a lack of standard methodology to characterize frequency responses of electric power grids for power line communication purpose. As a result, fair comparisons among measurement campaigns carried out in different parts of the world are missing. Aiming at to deal with this issue, this contribution discusses a complete sounding-based methodology to estimate frequency responses of electric power grids combining sampling frequency offset error estimation and correction, timing synchronization, channel estimation, and channel estimation enhancement techniques. The effectiveness of this methodology is validated by using well-known power line channel models, as well as measured ones, covering the frequency band from 1.7 up to 50 MHz. The attained results show that the methodology provides estimates in shorten period of time in comparison with the network analyzer based methodology and because of that it is capable of characterizing the periodically and time-varying behavior of electric power grids. Additionally, it is shown that the methodology can be successfully applied to characterize frequency responses of electric equipment and, as a consequence, it is very useful for both power line communication and power system applications.

Keywords Power grids · Frequency response · Estimate enhancement

T. R. Oliveira (✉)
IFSEMG, Juiz de Fora, MG, Brazil
e-mail: thiago.oliveira@ifsudestemg.edu.br

C. A. G. Marques · W. A. Finamore · M. V. Ribeiro
UFJF, Juiz de Fora, MG, Brazil
e-mail: cristiano.marques@engenharia.ufjf.br

W. A. Finamore
e-mail: finamore@ieee.org

M. V. Ribeiro
e-mail: mribeiro@ieee.org

S. L. Netto
UFRJ, Rio de Janeiro, RJ, Brazil
e-mail: sergioln@smt.ufrj.br

1 Introduction

Aiming at to fulfill the telecommunication demands related to Smart Grids, the electric power grids are being considered for data communication. The technology that makes use of the electric power grids as communication media is called power line communication (PLC) (Gotz et al. (2004)). Then, the knowledge and understanding of such communication media are of utmost importance to design of reliable and efficient PLC technologies that deal with the hardness and limitations of a media that were developed to transmit a huge amount of energy at very low frequency (50 Hz or 60 Hz). In this regards, it is well known that the channel frequency response (CFR) of a data communication medium is one of the most relevant information because it defines the strategy to deal with the impairments in such a kind of data communication media. Based on the CFR, several features can be extracted, such as average channel gain, coherence bandwidth, coherence time, theoretical channel capacity, and root mean squared delay spread (RMS-DS).

The CFR estimation methodologies for data communication purpose (in which the considered frequency bandwidth is much broader than the mains frequency) can be grouped into two approaches: (i) vectorial network analyzer (VNA): where the frequency response is estimated from the S-parameters (Tlich et al. 2008); (ii) sounding: where the frequency response is estimated by signal generation and

acquisition equipments together with signal processing tools (Parsons et al. 1991).

The first class, due to its simplicity, has been widely applied to estimate CFR in homes and vehicles (Tlich et al. 2008; Taherinejad et al. 2012; Tonello et al. 2014; Gassara et al. 2014) because the distances from the injecting and extracting points are short. However, the use of VNA-based approach can result in wrong estimates of the CFR because it demands a time interval (sweep time) higher than 100 ms to yield one estimate of the CFR while the coherence time T_c, time interval in which the channel impulse response is time invariant, of electric power grids is lower than 2 ms (Corripio et al. 2006; Picorone et al. 2014).

On the other hand, the sounding approach is more suitable for estimating CFRs because the time interval required to provide one measure of the CFR can be made lower than the coherence time by choosing data generation and acquisition equipments and changing some parameters of the signal processing tools considered in the sounding approach. Also, this approach can offer improved performance if the distances are long, such as in outdoor low-, medium-, and high-voltage electric power grids.

Regarding the sounding approach, a technique that only estimates the amplitude spectrum of a CFR, which is based on spectrum analyzer, was discussed in Mingyue (2006). A brief description of a channel estimation technique was addressed in Corripio et al. (2006). The use of signal generation and acquisition equipment together with sounding technique based on an orthogonally frequency division multiplexing (OFDM) for estimation CFR was addressed in Zimmermann and Dostert (2002); Barmada et al. (2010). The weakness of these contributions is the fact that few attentions are driven to the following issues altogether: (i) the choice of channel estimation technique; (ii) the choice of timing synchronization technique; (iii) the design of sampling frequency offset (SFO) correction technique; and (iv) the use of a channel estimation enhancement technique. In fact, the majority of contributions pays more attention to the characterization of communication media than on the applied methodologies (Tonello et al. 2014; Gassara et al. 2014). A first tentative to provide a reasonable and useful description of a methodology for estimating CFR in electric power grids was presented in Oliveira et al. (2013). However, a contribution that presents a reliable and easy to use methodology for estimating CFR by addressing the four aforementioned issues is missing in the literature. As a result, fair comparisons among measurements carried out in different parts of the world can not be correctly analyzed. Also, some contradictory information regarding the characterization of electric power grids as communication media have appeared (e.g., lognormality discussion about the average channel gain (Tonello et al. 2014; Galli et al. 2010). Therefore, it is of utmost importance to introduce a CFR estimation methodology that could be worldwide used.

Aiming at to deal with this issue, this contribution discusses a complete sounding-based methodology for estimating CFR of electric power grids for data communication purposes. The novelty is the effective combination of SFO error estimation and correction, timing synchronization, channel estimation, and channel estimation enhancement techniques. In this regard, the presented methodology discusses a comprehensive description of an OFDM-based sounding approach by addressing sampling frequency offset (SFO) error estimation and correction, timing synchronization, channel estimation, and channel estimation enhancement techniques. The effectiveness of this methodology is validated by well-known power line channel models, as well as measured ones, covering the frequency band from 1.7 up to 50 MHz. Measurement results show that the presented methodology is capable of offering one estimate of PLC channels per time interval as low as $T_f = 23.4\ \mu s$ for the chosen sampling frequency. As a result, it is possible to characterize periodically and time-varying behaviors of electric power grids because $T_f < T_c$ (T_c is the coherence time), something that is impossible to be achieved by a VNA. Additionally, it is shown that the methodology can be successfully applied to characterize the frequency responses of electric equipment and, as a consequence, it is very useful for both power line communication and power system applications.

To introduce all these technical contributions, this work is organized as follows: Sect. 2 describes the problems related to the PLC-channel frequency response estimation. Section 3 gives a detailed description of the proposed methodology. In Sect. 4, the frequency-estimation results are shown, whereas Sect. 5 draws the work conclusions.

2 Problem Formulation

For illustration purposes, the measurement setup used for PLC channel measurement (Philipps (1998)) is depicted in Fig. 1. In this scenario, the received signal $y(t)$ can be modeled by

$$y(t) = \tilde{y}(t) + v(t) = \int_{-\infty}^{\infty} x(\tau) h_{\text{eq}}(t, \tau) d\tau + v(t), \qquad (1)$$

in which $h_{\text{eq}}(t, \tau)$ is the linear and time-varying channel impulse response and $v(t)$ is the additive noise. The function $h_{\text{eq}}(t, \tau)$ accounts for all the linear filtering to which the signal $x(t)$ is subject and the noise term $v(t)$ includes all the perturbations that affect the communication channel. We assume that $y[n] = y(t)|_{t=nT_s} = \tilde{y}[n] + v[n]$, where $T_s \geq \frac{1}{2B}$.

Note that $h_{\text{eq}}(t, \tau)$ addresses the time-varying channel model that is composed of the front/end of the transceiver

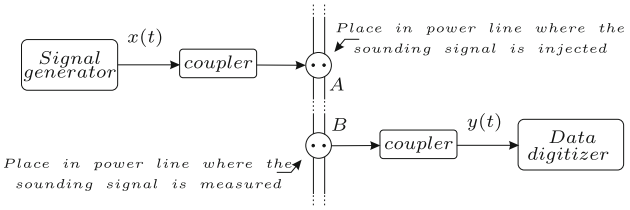

Fig. 1 Measurement setup

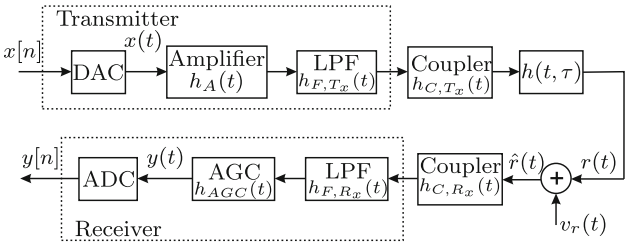

Fig. 2 PLC channel model

and the communication medium, see Fig. 2. In this plot, the boxes are labeled with $h_A(t)$, $h_{F,T_x}(t)$, $h_{F,R_x}(t)$, $h_{C,T_x}(t)$, $h_{C,R_x}(t)$, $h_{AGC}(t)$, and $h(t,\tau)$, which correspond to the impulse-response functions of the amplifier, transmitter and receiver low pass filter (LPF), transmitter and receiver couplers, automatic gain control (AGC), and the PLC channel, respectively. It is important to notice the bandwidth-limiting role of both LPFs which are intended to limit the signal bandwidth to B Hz. For a compact notation, we consider $h_T(t) = h_A(t) \star h_{F,T_x}(t) \star h_{C,T_x}(t)$ and $h_R(t) = h_{C,R_x}(t) \star h_{F,R_x}(t) \star h_{AGC}(t)$, where $\star$ denotes the linear-convolution operation and we assume that $h_{eq}(t,\tau) = h_{eq}(t-\tau)$ because the CFR estimation is carried out in a time interval lower than T_c. The analog signal $y(t) = \tilde{y}(t) + v(t)$, where $\tilde{y}(t) = x(t+T_d) \star h_T(t+T_d) \star h(t)$ and $v(t) = v_r(t) \star h_R(t)$. Also worth emphasizing is that the delay T_d, which the channel adds to the transmitted signal, is unknown to the receiver and, for this reason, has to be estimated *a priori* to any processing (timing synchronization).

Now, suppose that, at the receiver side, a perfect timing synchronization has been achieved, and that after the cyclic prefix (it is assumed that the OFDM with cyclic prefix signal is used as sounding signal, as detailed in Sect. 3.1) has been removed, we are left with the vectors of samples of the form $\mathbf{y}_i \in \mathbb{R}^{2N\times 1}$. By considering $h_{eq}[n] = h_T(t) \star h(t) \star h_R(t)|_{t=nT_s}$ and using the notation $\mathbf{h}_{eq} = \{h_{eq}[0]\ h_{eq}[1]\ \ldots\ h_{eq}[L_{eq}-1]\}^T$, it can be written $\mathbf{H}_{eq} = (1/\sqrt{2N})\mathbf{W}\{\mathbf{h}_{eq}^T\ \ \mathbf{0}_{2N-L_{eq}}^T\}^T$, where the superscript ^{T} denotes the transpose operation. Similarly, by considering $h_R[n] = h_R(t)|_{t=nT_s}$ and using the notation $\mathbf{h}_R = [h_R[0]\ \ h_R[1]\ \ \ldots\ \ h_R[L_R-1]]^T$, we can write that $\mathbf{H}_R = (1/\sqrt{2N})\mathbf{W}[\mathbf{h}_R^T\ \ \mathbf{0}_{2N-L_R}^T]^T$. Thus, by defining the matrix $\mathcal{H}_{eq} = \mathbf{diag}\{H_{eq}[0], \ldots, H_{eq}[2N-1]\}$ and $\mathcal{H}_R = \mathbf{diag}\{H_R[0], \ldots, H_R[2N-1]\}$, one can write that

$$\mathbf{Y}_i = \frac{1}{\sqrt{N}}\mathbf{W}\mathbf{y}_i = \mathcal{H}_{eq}\mathbf{X}_i + \mathcal{H}_R\mathbf{V}_r. \tag{2}$$

Considering that the zero-forcing criterion is used and with $\mathbf{X}_i = \{X_i[0], X_i[1], \ldots, X_i[2N-1]\}^T$, the OFDM input symbol, known *a priori* by the receiver, the following channel estimate is obtained:

$$\hat{\mathbf{H}}_{eq} = \left[\mathrm{diag}(\mathbf{X}_i)\right]^{-1}\mathbf{Y}_i = \mathbf{H}_{eq} + \left[\mathrm{diag}(\mathbf{X}_i)\right]^{-1}\mathcal{H}_R\mathbf{V}_r. \tag{3}$$

At this point, a few comments related to the estimation problem must be emphasized

- A careful choice of $\mathbf{X}_i$ is fundamental to render a useful estimation of the PLC CFR, a reduced peak to average power ratio, and a improved timing synchronization.
- A proper estimation of T_d must be achieved to avoid interblock interference.
- A proper SFO error estimation and correction is needed to avoid the degradation of the estimates.
- a signal enhancement technique is demanded to reduce the hardness of disturbances in the electric power grids.

3 The Methodology for Channel Frequency Response Estimation

The CFR estimation methodology involves the following issues, to be detailed in the subsequent subsections:

- Signal generation;
- Timing synchronization;
- Sampling frequency offset error estimation and correction;
- Channel estimation;
- Channel estimation enhancement.

3.1 Signal Generation

The modulated signal $x(t)$ chosen to be transmitted is an OFDM signal, occupying a bandwidth of B Hz. The OFDM variation called Hermitian symmetric OFDM (HS-OFDM) (da Costa Pinto et al. 2011) is adopted here as the baseband transmission modulation scheme, as represented in Fig. 3. In this scheme, the modulated data are submitted to a serial-to-parallel converter that outputs the vector $\mathbf{X}_i \in \mathbb{C}^{N\times 1}$ next mapped into a vector, denoted by $\mathbf{X}_{map,i} = \{X_{map,i}[0],\ X_{map,i}[1],\ \ldots\ ,\ X_{map,i}[2N-1]\}^T$, according to the following rule

$$X_{map,i}[k] = \begin{cases} \Re\{X_i[N-1]\}, & k=0 \\ X_i[k], & k=1,\ldots,N-2 \\ \Im\{X_i[N-1]\}, & k=N-1 \\ X_i^*[2N-2-k], & k=N, N+1,\ldots,2N-1 \end{cases}, \tag{4}$$

in which $\Re\{.\}$ and $\Im\{.\}$ denote the real and imaginary parts, respectively, of a given number, and * denotes the complex-conjugation operation.

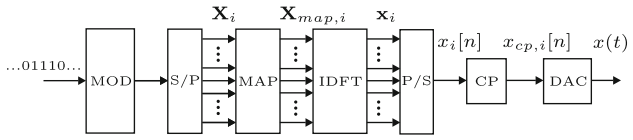

Fig. 3 HS-OFDM transmission system

To complete the HS-OFDM generation process, a L_{cp}-length cyclic prefix (CP) is inserted in each OFDM symbol. To this end, let us consider $\mathbf{x}_i = \frac{1}{\sqrt{2N}}\mathbf{W}^{\dagger}\mathbf{X}_{map,i}$, where $\mathbf{X}_{map,i} \in \mathbb{R}^{2N\times 1}$ is the frequency domain representation of the i^{th} HS-OFDM symbol, the matrix $\mathbf{W}$ is the $2N \times 2N$ discrete Fourier Transform (DFT) matrix and (†) the Hermitian operator. We have then, by pre-appending the CP, the vector with the last L_{cp} coefficients of $\mathbf{x}_i$, we get $\mathbf{x}_{cp,i} = \{x_i[2N-L_{cp}]\, x_i[2N-L_{cp}+1] \ldots x_i[2N-1]\, \mathbf{x}_i^T\}^T$.

Following this framework, the input signal to the channel is the infinite succession of HS-OFDM symbols represented in the discrete time-domain by

$$x_{cp}[n] = \sum_{i=-\infty}^{\infty} \sum_{j=0}^{N+L_{cp}-1} x_{cp,i}[j]\delta[n - i(N + L_{cp}) - j], \tag{5}$$

in which $\delta[\ell]$ is the Kronecker delta function, with unitary value for $\ell = 0$ and null for all other values of ℓ. $T_f = (N + L_{cp})T_s$ is the period of the HS-OFDM symbol ($T_f < T_c$). Also, $x_{cp,i}[j]$ is the j^{th} coefficient of the vector $\mathbf{x}_{cp,i}$.

3.2 Synchronization

In possession of the sequence $\{y[n]\}$, of length L_y,that represents the discrete signal measured at the PLC channel output, the timing synchronization process is performed. It is applied to each portion of the auxiliary sequence defined as $\{y_j[n]\} = \{y[n + \Delta]\}_{n=0}^{L_j-1}$, where Δ is varied until all the sequence $\{y[n]\}$ is analyzed and L_j denotes the length of the sequence $\{y_j[n]\}$ which must be properly chosen to include an entire HS-OFDM symbol. The aim of this step is to identify the initial sample of each HS-OFDM transmitted symbol. The synchronization task is based on the CP redundancy incorporated to the HS-OFDM symbol (Keller and Hanzo (1996)), which can be detected through the correlation between the vectors $\mathbf{y}_{1,l} = \{y_j[l] \;\; y_j[l+1] \;\; \ldots \;\; y_j[l + L_{cp} - 1]\}^T$ and $\mathbf{y}_{2,l} = \{y_j[l + 2N] \;\; y_j[l + 2N + 1] \;\; \ldots \;\; y_j[l+2N+L_{cp}-1]\}^T$. Thus, by defining the correlation vector as $\mathbf{y}_{corr} = [y_{corr}(0) \;\; y_{corr}(1) \;\; \ldots \;\; y_{corr}(L_j - (2N + L_{cp} + 1))]^T$, one has that

$$y_{corr}[l] = \langle \mathbf{y}_{1,l}, \mathbf{y}_{2,l} \rangle = \mathbf{y}_{1,l}^T \mathbf{y}_{2,l}, \tag{6}$$

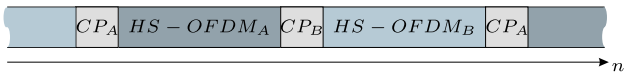

Fig. 4 Transmitted signal

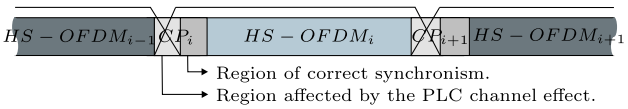

Fig. 5 Region in which the synchronism is considered correct

where the symbol $\langle \cdot, \cdot \rangle$ denotes the inner product operator and l is the l^{th} shift of the vectors $\mathbf{y}_{1,l}$ and $\mathbf{y}_{2,l}$.

To ensure that the synchronization step works properly, it is suggested that the transmitted frame assumes the profile indicated in Fig. 4. In that case, the transmitted signal is composed of two different HS-OFDM symbols, periodically transmitted. This configuration provides a delay and a channel estimation for each HS-OFDM symbol, with the receiver requiring only the two HS-OFDM originally sent symbols.

Consider that the initial estimation of the synchronism point, which indicates the initial sample of an HS-OFDM symbol within the sequence $\{y_j[n]\}$ (the samples that comprise the CP are exuded) is given by

$$l_{sync} = l_{\max} + L_{cp} = \arg\max_{l} (y_{corr}[l]) + L_{cp}. \tag{7}$$

The signal transmitted over the channel suffers a time scattering that is related to the channel impulse response spread. This phenomenon introduces interblock interference (IBI) and affects the synchronization process. If $L_{cp} \geq L_{eq}$ there is a region that can be considered as the beginning of the HS-OFDM symbol. In other words, the synchronization is correct if l_{sync} is within the interval depicted in Fig. 5.

In practice, it is observed that the synchronism estimate, as derived in (7), is highly affected by channel noise and scattering effect. To circumvent this weakness, we propose the use of the metric defined as

$$m_t[r] = \frac{1}{K_d} \sum_{p=1}^{K_d} \left[y_j\left(l_{sync} - \frac{R}{2} + r - p\right) - y_j\left(l_{sync} - \frac{R}{2} + 2N + r - p\right) \right]^2, \tag{8}$$

where $r = 0, 1, \ldots, R-1$. Actually, (8) evaluates the mean square error of K_d samples that precede the l_{sync}^{th} sample with its correspondent samples displaced by $2N$ samples, similar to the metric introduced in Beek et al. (1999). This calculation is taken over the interval $l_{sync} - R/2 \leq l_{sync} \leq l_{sync} + R/2$, where $R \in \mathbb{Z}$. Therefore, it can be observed that low-valued coefficients within $\mathbf{m}_t = \{m[0]\; m[1] \; \ldots \; m[R-1]\}^T$, where l_{sync} is found, are in the region of the correct synchronism. These values tend to increase when l_{sync} moves into the signal HS-OFDM from the boundary defined by the CP. Thus,

a new synchronization point can be defined as $l'_{sync} = l_{sync} - \arg \min_r\{m_t[r]\}$, where the term $\arg \min_r\{m_t[r]\}$ corresponds to the lowest coefficient of the vector $\mathbf{m}_t$.

After the starting point of a HS-OFDM symbol is estimated, within the current sequence $\{y_j[n]\}$, a shift of Δ samples is performed in order to get the forthcoming sequence $\{y_{j+1}[n]\}$. The initial sample of the i^{th} HS-OFDM symbol in the sequence $\{y[n]\}$ can be represented by $n'_{sync,i} = l'_{sync} + \Delta$, where $i = 0, 1, ..., K-1$ and K is the number of obtained estimates.

As a final step in the synchronization process, we average all starting points $n'_{sync,i}$, $i = 0, 1, ..., K-1$, of the K HS-OFDM symbols to mitigate the effect of noisy interferences, and the final synchronism point is determined as

$$\hat{n}_{sync} = \frac{1}{K}\sum_{i=0}^{K-1} n'_{sync,i} - \big(i(2N + L_{cp})\big). \tag{9}$$

This simple averaging procedure, combined with the correlation-based estimate, effectively substitutes a more elaborated estimation procedure, such as the ones based on the maximum likelihood (ML) algorithm (Beek et al. 1997) or the minimum mean squared error (MMSE) algorithm (Chevillat et al. 1987).

3.3 Channel Estimation

Once $\hat{n}_{sync}$ is defined, we obtain the vectors $\mathbf{y}_{med,i} = \{y_{med,i}[0], y_{med,i}[1], ..., y_{med,i}[2N-1]\}^T$, in which $y_{med,i}(j) = y[\hat{n}_{sync} + i(2N + L_{cp}) + j]$, $i = 0, 1, ..., K-1$ and $j = 0, 1, ..., 2N-1$, comprising the samples of the i^{th} HS-OFDM symbol not including the CP samples.

The problem remaining is to select which HS-OFDM symbol, either A or B, the vector $\mathbf{y}_{med,i}$ belongs to. Let the vectors $\mathbf{x}_i \in \mathbb{R}^{2N\times 1}$ be the distinct HS-OFDM transmitted symbols. As the transmitted signal has two different HS-OFDM symbols in it, we can now calculate the correlations operations $corr_{A,i} = \langle \mathbf{x}_A, \mathbf{y}_{med,i}\rangle$ and $corr_{B,i} = \langle \mathbf{x}_B, \mathbf{y}_{med,i}\rangle$ and state the following decision rule:

If $corr_{A,i} > corr_{B,i}$, then the vector $\mathbf{y}_{med,i}$ corresponds to the symbol HS-OFDM$_A$;

Else if $corr_{A,i} < corr_{B,i}$, then the vector $\mathbf{y}_{med,i}$ corresponds to the symbol HS-OFDM$_B$;

Else if $corr_{A,i} = corr_{B,i}$, then the vector $\mathbf{y}_{med,i}$ is discarded.

Let the i^{th} CFR estimate designated by $\hat{\mathbf{H}}_{eq,i} = \hat{H}_{eq,i}[0], \hat{H}_{eq,i}[1], \ldots, \hat{H}_{eq,i}[2N-1]^T$. With the notation $\mathbf{Y}_{med,i} = (1/\sqrt{2N})\,\mathbf{W}\mathbf{y}_{med,i}$ and $\mathbf{X}_{map,i} = (1/\sqrt{N})\,\mathbf{W}\mathbf{x}_i$, by applying the zero-forcing criterion, we thus have that

$$\hat{\mathbf{H}}_{eq,i} = \big[\mathrm{diag}(\mathbf{X}_{map,i})\big]^{-1}\mathbf{Y}_{med,i}. \tag{10}$$

3.4 Channel Estimation Enhancement

The effects of additive channel noise on the frequency-response estimates given by (10) can be significantly reduced by deploying the procedure described as follows.

The estimate of the CFR can be rewritten as $\mathcal{H}_{eq} = \sqrt{2N}\mathrm{diag}\{\mathbf{F}_{2N,2N}\mathbf{h}_{eq,ext}\}$, where $\mathbf{F}_{2N,2N}$ is the $2N \times 2N$ matrix with $2N > L_{eq}$, that is applied to the inverse discrete Fourier transform (IDFT), and $\mathbf{h}_{eq,ext} = \{h[0], h[1], \ldots, h[L_{eq}-1], 0, \ldots, 0\}^T$ is the extended version of the channel impulse response with $2N - L_{eq}$ zeros appended.

If the received signal is corrupted by the additive noise, the last coefficients in the channel impulse response, derived from the IDFT of (10), should be different from zero. Assuming that the length of the impulse response is such that $L_{eq} < L_{cp} \ll 2N$, then it becomes clear that the last samples of the estimated channel impulse response are just noisy coefficients that can be disregarded (Cardoso et al. (2009)) to attain a more reliable estimate. Since, in practice, the true value of L_{eq} is unknown, a reasonable assumption here is to consider $L_{eq} = L_{cp}$. The matrix $\mathbf{W}_o$ that projects a given $2N$-length vector onto this L_{cp}-dimension subspace is given by $\mathbf{W}_o = \mathbf{F}_{2N,L_{cp}}(\mathbf{F}^{\dagger}_{2N,L_{cp}}\mathbf{F}_{2N,L_{cp}})^{-1}\mathbf{F}^{\dagger}_{2N,L_{cp}}$, where $\mathbf{F}_{2N,L_{cp}}$ is a $2N \times L_{cp}$ matrix containing the first L_{cp} columns of the $2N$-point DFT matrix. Thus, an improved channel estimate for the i^{th} CFR is given by

$$\hat{\mathbf{H}}^{w}_{eq,i} = \mathbf{W}_o\hat{\mathbf{H}}_{eq,i}. \tag{11}$$

3.5 Sampling Frequency Offset Error Estimation and Correction

When the frequency of the clock in the signal generator and the acquisition equipment are different then sampling frequency offset (SFO) error occur. The SFO can result insevere degradation of the estimates, as discussed in Chiueh and Tsai (2007). When the distances between the ejecting and the extracting points are short, a cable can be used in order to guarantee the same clock in both transmitter and receiver equipments. On the other hand, for large distances some signal processing tools must be applied to estimate the SFO and provide its correction.

The SFO can be estimated from two consecutive received OFDM symbols, using

$$\mathrm{SFO}_{error} = \frac{1}{2N + L_{cp}}\left(\arg\max_s\left\{|\hat{h}^{w}_{eq,i+1}[s]|\right\} - \arg\max_s\left\{|\hat{h}^{w}_{eq,i}[s]|\right\}\right), \tag{12}$$

where $s = 0, 1, ..., 2N-1$. Also, the estimate of the SFO_{error} can be enhanced by averaging the values in a vector ϵ where each coefficient corresponds to the error from each pair of consecutive CIRs, and is now defined as $\mu_{SFO_{error}}$.

Based on the $\mu_{SFO_{error}}$ value, a new sequence $\{z[n]\}$ can be obtained through a interpolation technique using (Gardner et al. 1993)

$$z[n] = \sum_{\lambda=0}^{L_p} \mu_n^{\lambda} \sum_{\varrho=0}^{I-1} b_{\lambda}[\varrho] y[m_n - \varrho], \tag{13}$$

where I is the number of taps if the interpolating filter is one of finite impulse response (FIR), L_p is the polynomial's degree, $b_{\lambda}[\varrho]$ are independent coefficients, $\mu_n = \left(1 - \mu_{SFO_{error}}\right) - m_n$, and $m_n = \lfloor n(1 - \mu_{SFO_{error}}) \rfloor$, in which $\lfloor x \rfloor = \max\{m \in \mathbb{Z} | m \leq x\}$ denotes the largest integer not exceeding x. The values of the coefficients $b_{\lambda}[\varrho]$ and the quantities L_p and I can be obtained in Erup et al. (1993). The procedure for SFO estimation and correction is summarized in **Algorithm 1**.

Note that the correction of the SFO error will be performed using the enhanced CIR estimates, $\hat{\mathbf{h}}_{eq,i}^{w}$, and will result in the signal $\{z[n]\}$. Then, the methodology is applied again, but the signal $\{y[n]\}$ is replaced for $\{z[n]\}$.

Algorithm 1: SFO error estimation and correction algorithm.

Data: $\{y[n]\}$,$\hat{\mathbf{h}}_{eq}^{w}$
Result: $\{z[n]\}$
Initialization: $i = 0, n = 0$;
while $i \leq K - 2$ **do**
  $\epsilon[i] = \frac{1}{2N+L_{cp}} \left(\arg\max_s \left\{ |\hat{h}_{eq,i+1}^{w}[s]| \right\} - \arg\max_s \left\{ |\hat{h}_{eq,i}^{w}[s]| \right\} \right)$;
  $i = i + 1$;
end
$\mu_{SFO_{error}} = \frac{1}{K-1} \sum_{i=0}^{K-2} \epsilon[i]$;
while $n \leq L_y - I$ **do**
  $z[n] = \sum_{\lambda=0}^{L_p} \left(\left(1 - \mu_{SFO_{error}}\right) - int\left[n(1 - \mu_{SFO_{error}})\right] \right)^{\lambda}$
  $\sum_{\varrho=0}^{I-1} b_{\lambda}[\varrho] y[m_n - \varrho]$;
  $n = n + 1$;
end

3.6 Trigger Source Circuit

The circuit shown in Fig. 6 can be used in cases when the channel variability with respect to the zero crossing of the power fundamental signal is analyzed. The component $U1$ is an opto-transistor that works as a switch that is closed every time that its polarization condition is satisfied. The signal $v_{out}(t)$ can be used as a trigger that starts the measurements performed by the data acquisition equipment. With this triggering device, the first estimation corresponds to the HS-OFDM symbol received immediately after the detection of a zero crossing fundamental signal. As a result, it is possible to correlate the CFR estimates of the PLC channel with the periodicity of the main voltage signal (50 or 60 Hz) of electric power grids.

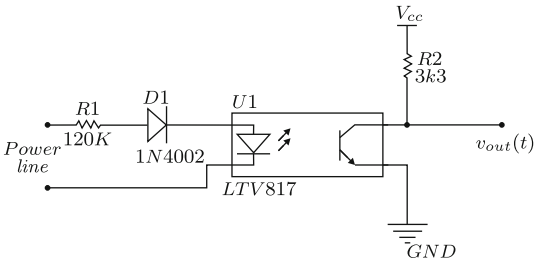

Fig. 6 Power line fundamental signal synchronization circuit

3.7 General Overview

The general structure of the algorithm for channel estimation, following all stages detailed above, is summarized in **Algorithm 2**.

4 Experimental Results

The results obtained using the presented methodology will have its discussion divided in three parts. In the first part, the performance of the presented methodology is evaluated using a well-known PLC channel model. In the second part, the methodology is analyzed on the measured data taken in real electric power grids. And finally, in the least part will be illustrated some results when considering the frequency response estimation of some electrical devices. In all cases, the adopted sampling frequency is 200 MHz and the analysis covers a frequency bandwidth from 1.7 up to 50 MHz to agree with the telecommunication regulation for PLC technology in Brazil (ANATEL (2009)). The transmitted signal features and adopted parameters are listed in Table 1. The number of symbols and the value L_j match with the requirement mentioned in Sect. 3.2, in order to ensure that the synchronization process works properly. The binary phase shift keying (BPSK) modulation was chosen due to its simple implementation and because it results in a very low peak to average power ratio (PAPR). The number of sub-carriers gives a frequency resolution of, approximately, 48.8 kHz, lower than the coherence bandwidth of indoor PLC channels. Furthermore, the symbol duration ($T = 23.04\,\mu s$) is made much less than 600 μs, which is the shortest coherence time of indoor PLC channels, according to Corripio et al. (2006). The length of the CP was chosen based on Martinez et al. (2010) in which the influence of this parameter was evaluated in more than 160 types of indoor PLC channels, measured in 20 different places. Finally, the last three parameters in Table 1 were heuristically chosen.

Algorithm 2: PLC channel estimation algorithm.

Data: $\{x[n]\}$,$\{y[n]\}$
Result: $\hat{\mathbf{H}}_i^w$
Initialization: $\Delta = 0, i = 0$;
while $\Delta \leq L - L_j$ **do**
  $\{y_j[n]\} = \{y[n+\Delta]\}_{n=0}^{L_j-1}$;
  for $l = 1, 2, ..., L_j - (2N + L_{cp} + 1)$ **do**
    $y_{corr}[l] = \langle \mathbf{y}_{1,l}, \mathbf{y}_{2,l} \rangle = \mathbf{y}_{1,l}^T \mathbf{y}_{2,l}$;
  end
  $l_{\max} = \arg\max_l (y_{corr}[l])$;
  $l_{sync} = l_{\max} + L_{cp}$;
  for $r = 0, 1, ..., R-1$ **do**
    $m_t[r] = \frac{1}{K_d} \sum_{p=1}^{K_d} \left[y_j\left(l_{sync} - \frac{R}{2} + r - p\right) - y_j\left(l_{sync} - \frac{R}{2} + 2N + r - p\right) \right]^2$;
  end
  $l'_{sync} = l_{sync} - \arg \min_n m_t[n]$;
  $n'_{sync,i} = l'_{sync} + \Delta$;
  $i = i + 1$;
  $\Delta = n'_{sync,i} + L_{cp}$
end
$\hat{n}_{sync} = \frac{1}{K} \sum_{i=0}^{K-1} n'_{sync,i} - (i(2N + L_{cp}))$;
$i = 0$;
while $i \leq K - 1$ **do**
  $\mathbf{y}_{med,i} = \Big\{ y\big[\hat{n}_{sync} + (i \times (2N + L_{cp}))\big], y\big[\hat{n}_{sync} + (i \times (2N + L_{cp})) + 1\big], ..., y\big[\hat{n}_{sync} + (i \times (2N + L_{cp})) + 2N - 1\big] \Big\}^T$;
  $corr_{A,i} = \langle \mathbf{x}_A, \mathbf{y}_{med,i} \rangle$;
  $corr_{B,i} = \langle \mathbf{x}_B, \mathbf{y}_{med,i} \rangle$;
  if $corr_{A,i} > corr_{B,i}$ **then** $\hat{\mathbf{H}}_{eq,i} = \left[\text{diag}(\mathbf{X}_{map,A})\right]^{-1} \mathbf{Y}_{med,i}$
  if $corr_{B,i} > corr_{A,i}$ **then** $\hat{\mathbf{H}}_{eq,i} = \left[\text{diag}(\mathbf{X}_{map,B})\right]^{-1} \mathbf{Y}_{med,i}$
  else the vector $\mathbf{y}_{med,i}$ is discarded
  $\hat{\mathbf{H}}_{eq,i}^w = \mathbf{W}_o \hat{\mathbf{H}}_{eq,i}$;
  $i = i + 1$;
end

4.1 Performance Analysis: PLC Channel Model

A simulated environment was used to evaluate the performance of the presented methodology. Table 2 summarizes the parameters of a well-known multipath PLC channel model that was used with this purpose, where g_i and d_i are, respectively, the gain and the length in meters associated with the i^{th} path. The magnitude of frequency response of this channel is depicted in Fig. 7a, while Fig. 7b shows its impulse response.

Figure 8 shows the values of the coefficients of the vector $\mathbf{m}_t$ that are used in the synchronization process. Notice that the position 80 refers to the initial estimation of the synchronization point (l_{sync}). Moreover, in Fig. 8, the region of correct synchronism, as discussed in Sect. 3.2 (see Fig. 5), can be easily observed as the one with smaller values for the coefficients of the vector

Table 1 Transmitted signal features and values of the parameters used by the PLC frequency response estimation algorithm

Number of HS-OFDM symbols	2
Modulation	BPSK
Number of sub-carriers	$N = 2048$
CP length	$L_{cp} = 512$
Symbol duration	$T_f = 23.04\,\mu s$
Length of the sequence $\{y_j[n]\}$	$L_j = 9216$
Number of samples used to compute $\mathbf{m}_t$	$K_d = 8$
Number of shift in the vector $\mathbf{m}_t$ calculus	$R = 128$
Number of symbols in the synchronism step	$K = 36$

Table 2 Parameters of an outdoor PLC channel model (Zimmermann and Dostert (2002))

i	1	2	3	4
g_i	0.64	0.38	−0.15	0.05
$d_i\,(m)$	200.00	222.40	224.80	267.50

$k = 1 \quad a_0 = 0 \quad a_1 = 7.8\ 10^{-10}$

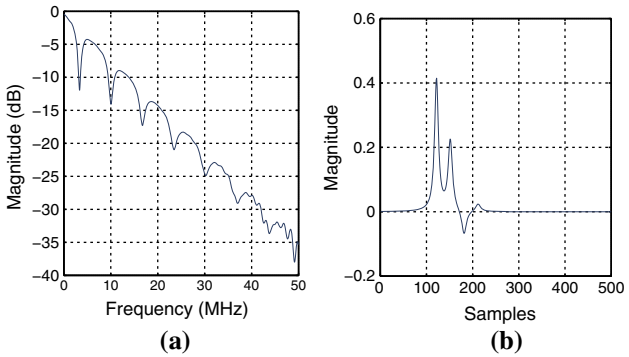

Fig. 7 Simulated PLC channel. **a** Magnitude function. **b** Impulse response

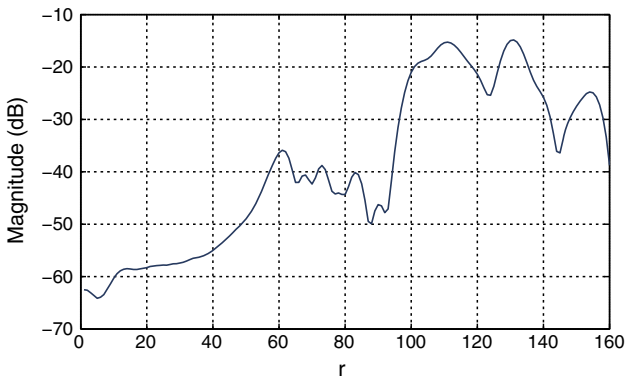

Fig. 8 Coefficients of the vector $\mathbf{m}_t$

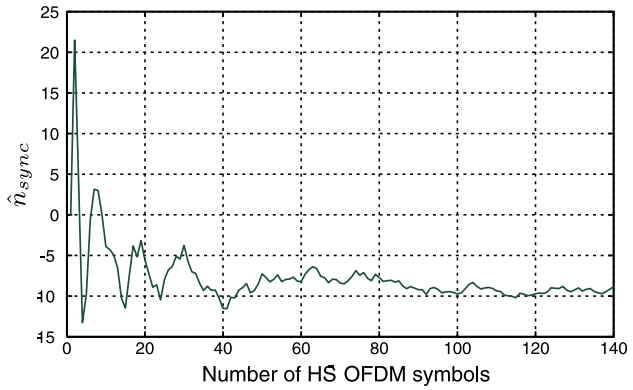

Fig. 9 Estimation of the correct synchronism point related to the number of HS-OFDM symbols

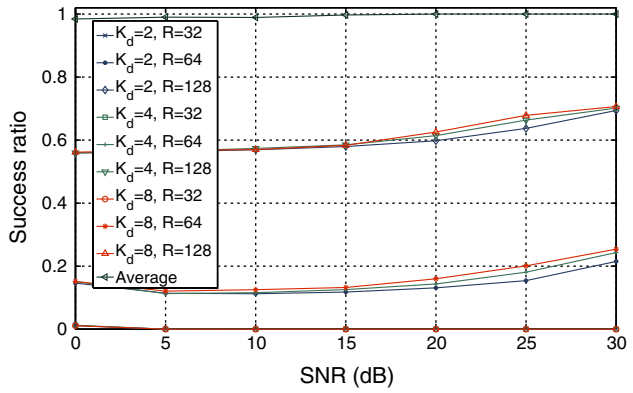

Fig. 10 Evaluation of the synchronism technique

Figure 9 shows as the average value of the synchronism point ($\hat{n}_{sync}$) varies with the number of considered HS-OFDM symbols. The vertical axis refers to the displacement of the estimated synchronism point with respect to the boundary defined by the CP. The positive values refer to the number of samples in that the synchronism point advances into the HS-OFDM symbol. On the other hand, negative values refer to the distance of the synchronism point to the ideal point (with value 0) into the CP. Notice that this last procedure plays a key role in the synchronization step, since individual estimates of the synchronism point can present a high error ratio (see Fig. 10).

The performance of the synchronism process is depicted in Fig. 10. In this case, the analysis was made with the signal transmitted through the PLC channel model and with additive white Gaussian noise (AWGN) by considering a signal-to-noise ratio (SNR) from 0 up to 30 dB, in steps of 5 dB. The simulation was taken over 1024 symbols for each SNR. The first number of the legend in the graphic is related to the K_d samples used when determining $\mathbf{m}_t$ and the second number refers to the shift R performed in the vector $\mathbf{m}_t$. As can be seen in this figure, for $R = 32$ the synchronism point is erroneously estimated within the symbol HS-OFDM almost all the time. For $R = 128$, the synchronism is correctly estimated more than 55% of the cases, reaching more than 70% for $K_d = 8$ and SNR = 30 dB The best result in Fig. 10, referred to as 'average' in the legend, is related to te last procedure of the synchronization step, given by Eq. (9), considering $K = 140$, $K_d = 2$ and $R = 128$.

Table 3 Mean MSE between the simulated and estimated CFR

Type of estimate	MSE (dB)
Single	−39.42
Mean of 2	−42.56
Mean of 4	−45.73
Mean of 8	−48.84
Mean of 16	−52.01
Single enhanced	−48.84

The improvement obtained with the use of the enhancement procedure was evaluated by considering the mean square error (MSE) metric. On that sense, the MSE between the simulated and estimated (with enhancement procedure) CFRs can be compared to the MSE between the simulated frequency response and the CFR estimated without the enhancement procedure. Furthermore, the comparison was made with respect to the MSE between the simulated frequency response and those from average of estimations (largely applied for noise interference mitigation, see Corripio et al. (2006). This comparison was made considering ideal synchronism condition. Results for several scenarios varying the SNR from 0 up to 30 dB, in steps of 5 dB, were examined (1024 channel estimations were taken for each scenario and the noise is the AWGN) and considering the average of 2, 4, 8, and 16 channel estimations – for the MSE calculus was taken 1024 averaged estimations for each SNR. Results for SNR equal to 20 dB are summarized in Table 3. It is important to notice that each time the amount of channel estimates used in the average is folded, the MSE is reduced by approximately 3 dB. On the other hand, the proposed enhancement procedure improves the estimation in almost 10 dB in all frequencies, which is very similar with the performance obtained to the average of 8 estimations. It is important to keep in mind that the larger the number of estimates greater the time interval from which it represents. Also, it is important to mention that similar improvements were observed in all tested SNRs and, furthermore, that the enhancement procedure has an important impact in the estimated frequency response of PLC channels. In fact, the enhanced estimate makes use of only one coarse estimate of the PLC CFR and results in a smooth and enhanced curve, as can be seen in Fig. 11 for the SNR equal to 20 dB.

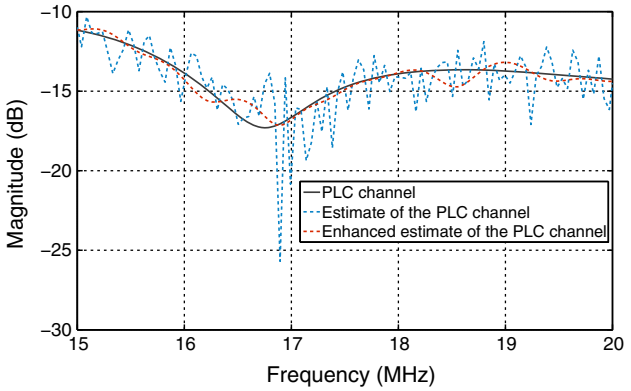

Fig. 11 Comparison of estimates with and without the proposed enhancement procedure

4.2 Performance Analysis: Real PLC Scenario

In this section, the results presented were obtained from measurements tacked in typical apartments in Brazil. The transmitter signal was generated offline and loaded into an arbitrary waveform generator system of 14 bits of resolution, and the receiver was a 16-bit digitizer, both equipments operating with the same clock frequency of 200 MHz. The clock in both equipments was forced through a cable be the same.

4.2.1 Comparison Between the Methodology and the VNA

In Fig. 12 is depicted the magnitude of two measured PLC channels. In both graphics are plotted the measures obtained by the presented methodology and the VNA (E5061B from Agilent). It is very important to highlight the differences between the measures. While the presented methodology gives an estimate each 23 μs, approximately, the VNA demands a time interval more than 300 ms, for a frequency resolution close to those presented by the methodology. So, one estimate of the PLC channel given by the VNA can represent distinct PLC channels in different frequency intervals. This must be the main reason for some discrepancies presented in Fig 12 between the estimates from the presented methodology and that one obtained with the VNA. Based on CFR estimates of real PLC channels it can be noted that the presented methodology can offer good results in comparison with the VNA.

4.2.2 Estimation of Real CFR

Figure 13 shows magnitude response of PLC channel in a typical apartment in Juiz de Fora, Brazil, as an example of the application of the presented methodology. This figure shows how CFRs can be different in an indoor electric power grids.

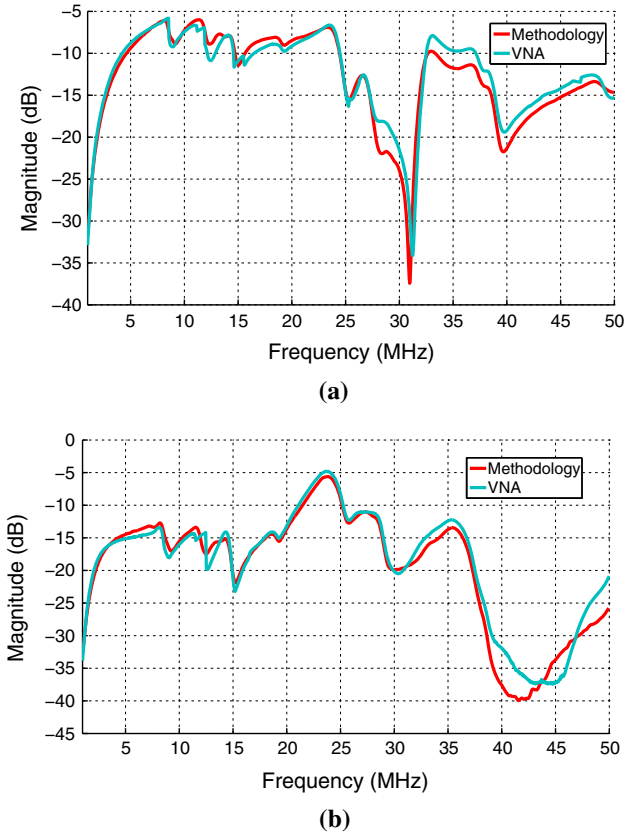

Fig. 12 CFR estimates of real PLC channels with the presented methodology and by using a VNA. **a** PLC channel #1. **b** PLC channel #2

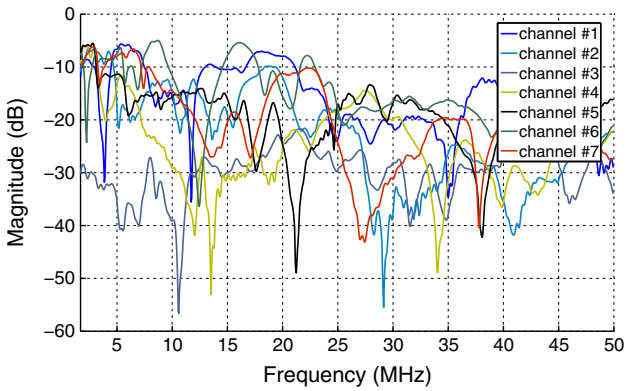

Fig. 13 Magnitude of the frequency response of seven measured PLC channels

In order to verify the performance of the presented methodology to estimate a periodically and time-varying PLC channel, a drill feeded by a source based on silicon controlled rectifier (SCR's) was connected in the power line under investigation. The estimate of the CFR can be seen in Fig. 14a, where the color bar denotes the channel gain in decibel and the measurement was triggered by the circuit of Fig. 6. As the main frequency in Brazil is 60 Hz, the changes

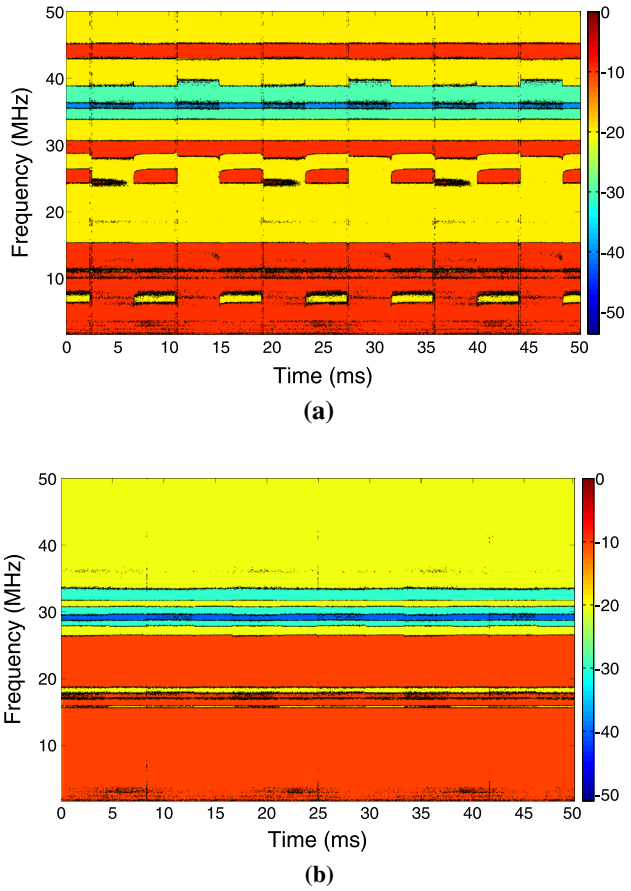

Fig. 14 Magnitude of CFR estimates of PLC channels. **a** Periodically time-varying PLC channel. **b** Time invariant PLC channel

occur approximately around every 8.33 ms (a half cycle of the main frequency). In the analyzed case, these behavior can be clearly verified in some frequencies around 6 and 27 MHz. Figure 14b shows the CFR of successive measures of time invariant PLC channels. These figures are composed of more than 2, 000 consecutive CFR. This is a kind of result that is impossible to be obtained with the VNA because its sweep time is higher than 300 ms.

4.3 Performance Analysis: Application on Electrical Devices

It is well known the applicability of the frequency response of electrical devices to support several analysis (Platero et al. 2011; Marek and Jakub 2004; Zhongdong et al. 2009). In order to illustrate the flexibility of the presented methodology, in Fig. (15) is portrayed the magnitude estimates of the CFR of some electrical devices. Again, the CFR estimates obtained through the methodology are compared with those from the VNA. In Fig. 15a the comparison is performed under the coupler circuity used to avoid damages in the equipments involved on the PLC channel measurements. It is clear its

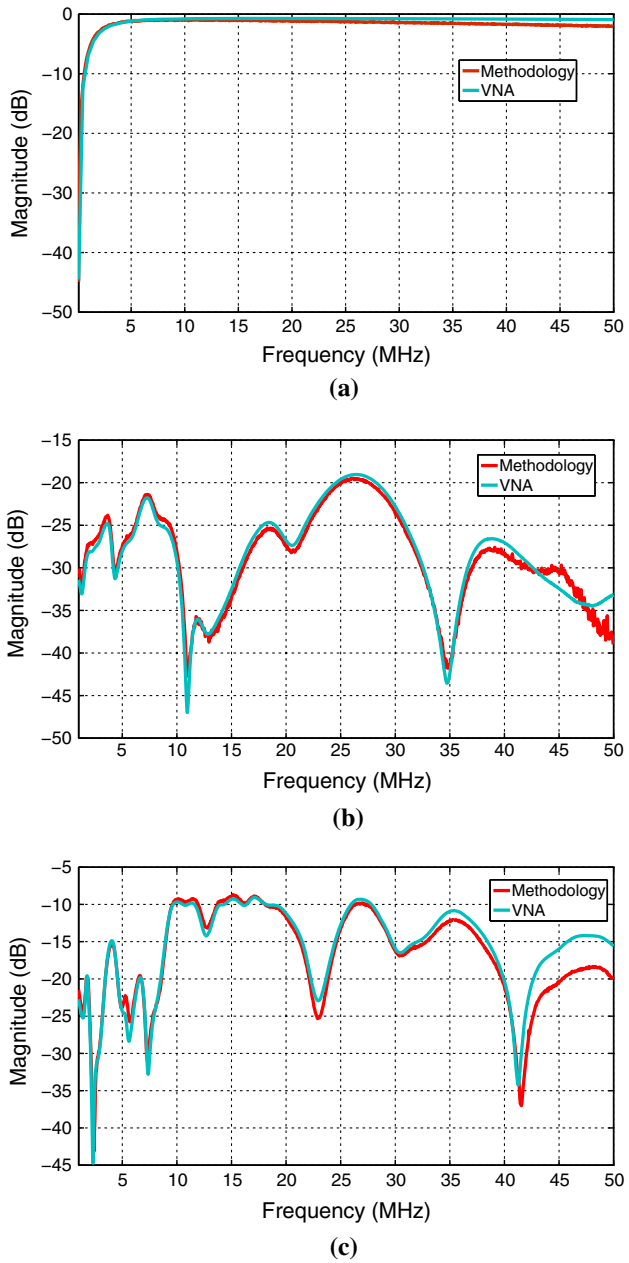

Fig. 15 Comparison between magnitude of the frequency response estimate obtained by the presented methodology and the VNA. **a** PLC coupler circuity **b** Transformer #1 **c** Transformer #2

behavior as a low pass filter, blocking the main voltage signal (50 or 60 Hz) of the power lines. Figures 15b and c shown the CFR of two monophasic transformers. The transformer #1 is of 18 VA while transformer #2 is of 1 kVA.

These plots show the effectiveness of the presented methodology because the estimate of the magnitude function present low differences in comparison with the VNA. This and several other comparisons confirm that the proposed methodology is useful for estimating CFR of the electric power grids and electrical devices.

5 Conclusion

This contribution detailed a complete methodology to estimate CFR of electric power grids for power line communication purposes. The presented methodology incorporates frequency sampling offset error estimation and correction, timing synchronization, channel estimation and channel estimation enhancement that improve the quality of the frequency response estimates. The reported results, based on both synthetic and measured data, showed the effectiveness of proposed methodology. By using PLC channel models, it was verified that all techniques in the methodology contribute to offer reliable estimates of CFR. Moreover, the presented methodology is capable of estimating CFR of both linear time invariant and linear and periodically time-varying PLC channels in low voltage and indoor electric power grids, while the VNA can only characterize linear time invariant PLC channels. The efficiency of the described methodology was corroborated by experimental results in which estimates of CFR of a PLC coupler and monophasic transformers were compared to estimates provided by a VNA. Based on the attained results, the presented methodology can be very useful for both power line communication and power system applications.

Acknowledgments The authors would like to thank to IFSEMG, FINEP, FAPEMIG, CNPq, CAPES, P&D ANEEL, CEMIG, CAPES/PNPD, INERGE and Smarti9 for their financial support.

References

ANATEL. (2009). Brazilian resolution for PLC. Retrieved January, 2014 http://legislacao.anatel.gov.br/resolucoes/2009/101-resolucao-527.

Barmada, S., Bellanti, L., Raugi, M., & Tucci, M. (2010). Analysis of power-line communication channels in ships. *IEEE Trans on Vehicular Technology*, *59*(7), 3161–3170.

Cardoso, D. F., Backx, F. D., & Sampaio-Neto, R. (2009). Improved pilot-aided channel estimation in zero padded MC-CDMA systems. In *International Symposium on Wireless Pervasive Computing*, (pp. 1–5).

Chevillat, P., Maiwald, D., & Ungerboeck, G. (1987). Rapid training of a voiceband data-modem receiver employing an equalizer with fractional-t spaced coefficients. *IEEE Trans on Communications*, *35*(9), 869–876.

Chiueh, T. D., & Tsai, P. Y. (2007). *OFDM Baseband Receiver Design for Wireless Communications*. Hoboken: John Wiley & Sons.

Corripio, F. J. C., Arrabal, J. A. C., del Rio, L. D., & Munoz, J. T. E. (2006). Analysis of the cyclic short-term variation of indoor power line channels. *IEEE Journal on Selected Areas in Communications*, *24*(7), 1327–1338.

da Costa Pinto, F., Scoralick, F. S. O., de Campos, F. P. V., Quan Z., & Ribeiro, M. V. (2011). A low cost OFDM based modulation schemes for data communication in the passband frequency. In *Proceedings of IEEE International Symposium on Power Line Communications and Its Applications*, (pp. 424–429).

Erup, L., Gardner, F. M., & Harris, R. A. (1993). Interpolation in digital modems. II. Implementation and performance. *IEEE Transactions on Communications*, *41*(6), 998–1008.

Galli, S. (2010). A simple two-tap statistical model for the power line channel. In *Proceedings of IEEE International Symposium on Power Line Communications and its Applications*, (pp. 242–248).

Gardner, F. M. (1993). Interpolation in digital modems. I. Fundamentals. *IEEE Transactions on Communications*, *41*(3), 501–507.

Gassara, H., Rouissi, F., & Ghazel, A. (2014). Statistical characterization of the indoor low-voltage narrowband power line communication channel. *IEEE Transactions on Electromagnetic Compatibility*, *56*(1), 123–131.

Gotz, M., Rapp, M., & Dostert, K. (2004). Power line channel characteristics and their effect on communication system design. *IEEE Communications Magazine*, *42*(4), 78–86.

Keller, T., & Hanzo, L. (1996). Orthogonal frequency division multiplex synchronisation techniques for wireless local area networks. In *Proceedings of IEEE International Symposium on Personal Indoor and Mobile Radio Communications*, (vol. 3, pp. 963–967).

Marek, F., & Jakub, F. (2004). Detection of winding faults in electrical machines using the frequency response analysis method. *Measurement Science and Technology*, *15*(10), 2067.

Martinez, S. J. J., Cortes, J. A., Diez, L., Canete, F. J., & Torres, L. M. (2010). Performance analysis of OFDM modulation on indoor PLC channels in the frequency band up to 210 MHz. In *Proceedings of IEEE International Symposium on Power Line Communications and Its Applications*, (pp. 38–43).

Mingyue, Z. (2006). Measurements and channel characteristics of LV power line communications networks in china. In *Proceedings of IEEE International Symposium on Power Line Communications and Its Applications*, (pp. 212–216).

Oliveira, T. R., Finamore, W. A., & Ribeiro, M. V. (2013). A sounding method based on OFDM modulation for PLC channel measurement. In *Proceedings of IEEE International Symposium on Power Line Communications and Its Applications*, (pp. 185–190).

Parsons, J. D., Demery, D. A., & Turkmani, A. M. D. (1991). Sounding techniques for wideband mobile radio channels: a review. *IEEE Proceedings in Communications, Speech and Vision*, *138*(5), 437–446.

Philipps, H. (1998). Performance measurements of power line channels at high frequencies. In *Proceedings of International Symposium on Power Line Communications and Its Applications*, (pp. 229–237).

Picorone, A. A. M., Neto, R. S., & Ribeiro, M. V. (2014). Coherence time and sparsity of brazilian outdoor plc channels: A preliminary analysis. In *Proceedings of IEEE International Symposium on Power Line Communications and its Applications*, (pp. 1–5).

Platero, C. A., Blazquez, F., Frias, P., & Ramirez, D. (2011). Influence of rotor position in FRA response for detection of insulation failures in salient-pole synchronous machines. *IEEE Transactions on Energy Conversion*, *26*(2), 671–676.

Taherinejad, N., Rosales, R., Lampe, L., & Mirabbasi, S. (2012). Channel characterization for power line communication in a hybrid electric vehicle. In *Proceedings of IEEE International Symposium on Power Line Communications and Its Applications*, (pp. 328–333).

Tlich, M., Zeddam, A., Moulin, F., & Gauthier, F. (2008). Indoor power-line communications channel characterization up to 100 MHz - Part I: One-parameter deterministic model. *IEEE Trans on Power Delivery*, *23*(3), 1392–1401.

Tonello, A. M., Versolatto, F., & Pittolo, A. (2014). In-home power line communication channel: Statistical characterization. *IEEE Transactions on Communications*, *62*(6), 2096–2106.

van de Beek, J. J., Sandell, M., & Borjesson, P. O. (1997). ML estimation of time and frequency offset in OFDM systems. *IEEE Trans on Signal Processing*, *45*(7), 1800–1805.

van de Beek, J. J., Borjesson, P. O., Boucheret, M. L., Landstrom, D., Arenas, J. M., Odling, P., et al. (1999). A time and frequency synchronization scheme for multiuser OFDM. *IEEE Journal on Selected Areas in Communications*, *17*(11), 1900–1914.

Zhongdong, W., Li, J., & Sofian, D. M. (2009). Interpretation of transformer FRA responses - part i: Influence of winding structure. *IEEE Transactions on Power Delivery*, *24*(2), 703–710.

Zimmermann, M., & Dostert, K. (2002). A multipath model for the powerline channel. *IEEE Trans on Communications*, *50*(4), 553–559.